MASSIVE STARS: THE PRE-SUPERNOVA EVOLUTION OF INTERNAL AND CIRCUMSTELLAR STRUCTURE

NORBERT LANGER
Institut für Physik, Universität Potsdam
Postfach 601553, D–14415 Potsdam, Germany
email: `ntl@astro.physik.uni-potsdam.de`

ALEXANDER HEGER
Max-Planck-Institut für Astrophysik
D–85740 Garching, Germany
email: `ahg@mpa-garching.mpg.de`

AND

GUILLERMO GARCíA-SEGURA
Instituto de Astronomia-UNAM, Apdo Postal 877
22800 Ensenada, B.C., Mexico;
email: `ggs@bufadora.astrosen.unam.mx`

Abstract. We review new developments in the theory of massive stars and their circumstellar environments, considering the evolution from the main sequence to the supernova explosion. Our focus is — for both aspects, the stellar interior and their immediate surroundings — to highlight recently explored effects of stellar rotation, in particular rotationally induced mixing of chemical species and of angular momentum, consequences for nucleosynthetic yields, the effect of rotation on the core collapse supernova mechanism, and the potential role of stellar rotation in shaping the circumstellar matter around B[e] stars, Luminous Blue Variable stars, and supernova progenitors.

1. Introduction

The quantitative theory of stellar structure is more than 100 years old (cf. Emden 1907). Our understanding of the stellar interior has improved dramatically during this time, especially so since it became possible to construct detailed stellar models with the help of computers, i.e. the 1950ies. Although still many fundamental questions are left in the field of low- and intermediate mass stars, we can say that their evolutionary path — i.e., their way from the main sequence through the red giant and asymptotic giant branch to the white dwarf stage — is know in detail since several decades (see, for example, Iben 1974). Also, the principles of the evolution of massive stars' cores through the major nuclear fusion stages from hydrogen to silicon burning are known for that long (cf. Weaver et al. 1978).

However, even today our understanding of the evolution of the observable properties of massive stars ($M_{\rm ZAMS} \gtrsim 8\ M_{\odot}, \log\ L/L_{\odot}\ \gtrsim 4$) is still rudimentary. For example, when in 1987 a *blue* supergiant exploded as a supernova in the Large Magellanic Cloud (cf. Arnett et al. 1989) it was a surprise to the community. Another example: the observed dependence of the blue-to-red supergiant ratio on metallicity contradicts *all* existing stellar evolution calculations (Langer & Maeder 1995). However, not only the post-main sequence phase of massive stars, even the core hydrogen burning evolution is sill poorly understood. As we shall discuss in detail below, the uncertainties in massive star evolution is dominated by the lack of understanding of two kinds of processes: the physics of mass loss from the stellar surface, and the physics of internal mixing processes (cf. Langer 1994). In the present paper, we want to outline that both processes, despite acting in quite different locations in massive stars, may be strongly influenced by a process which has been neglected in past studies of massive star evolution: rotation.

1.1. INSTABILITIES

Due to their huge luminosities a large fraction of the interior of massive stars is subject to hydrodynamic instabilities, even without considering rotation. E.g., for more than 20 years, a long debate in the astrophysical literature discussed the question whether the Schwarzschild or the Ledoux criterion for convection is the correct one — which, although rather irrelevant for low mass stars, is of vigorous importance for massive stars already on the main sequence (Stothers and Chin 1975, 1976). Even though first principles clearly lead to the Ledoux criterion, the Schwarzschild criterion — which ignores mean molecular weight gradients, is mostly used in evolutionary calculations for massive stars. This has been justified by the finding of an instability by Kato (1966) for layers in a star for which the Ledoux criterion predicts stability but which are super-adiabatic — i.e. unstable according to the Schwarzschild criterion. However, this instability, semiconvection, grows only on the local thermal time scale rather than on the dynamical time scale, and it should therefore not be treated in the same way as convection (Langer et al. 1983, 1985).

The possible local instabilities in a *non-rotating* star are schematically shown in Fig. 1, where the plane defined by the two stabilizing factors, sub-adiabaticity $\nabla_{\rm ad} - \nabla$ and molecular weight gradient ∇_μ, is divided into four regions. (As usual, $\nabla := \frac{d\ln T}{d\ln P}$, $\nabla_{\rm ad} := \left(\frac{\partial \ln T}{\partial \ln P}\right)_{{\rm s},\mu}$, and $\nabla_\mu := \frac{d\ln T}{d\ln \mu}$; cf. Kippenhahn & Weigert 1990). Note that in order to obtain stability, *both* factors have to be positive, i.e. act stabilizing. If only one of them is negative, an instability occurs. Note also that in order to obtain convection, it is not required that both factors are destabilizing. Rather, the stabilizing action of one of them can be compensated if the other is sufficiently strong and destabilizing. “Sufficiently strong” is defined here by the Ledoux criterion (cf. Fig. 1).

If the destabilizing factor is not sufficiently strong, the resulting instability obtains a character completely different from that of convection. When a mean molecular weight gradient stabilizes a super-adiabatic stratification, the resulting instability — semiconvection — is oscillatory, and it grows only on the thermal time scale. When an unstable μ-stratification — i.e., heavy particles are above lighter ones — is stabilized by sub-adiabaticity, we obtain a secular instability called thermohaline mixing, as it has been discussed first by oceanographers (cf. Huppert & Turner 1981). Also this instability grows only on the local thermal time scale.

During the last years, there is growing evidence that stellar rotation may con-

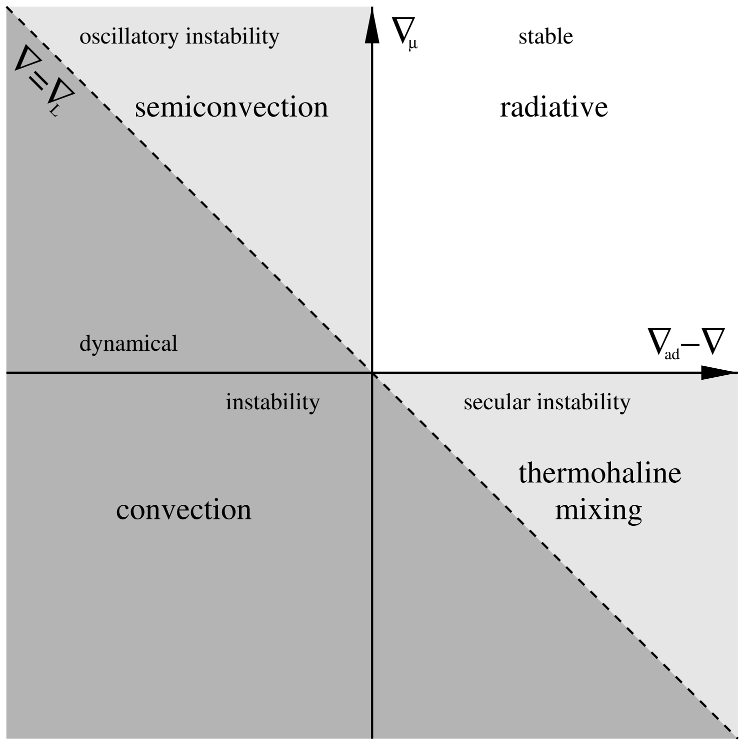

Figure 1. Schematic representation of possible local instabilities in a non-rotating, non-magnetic star. The stabilizing quantities sub-adiabaticity ($\nabla_{\rm ad} - \nabla$, i.e. $(\partial \ln T/\partial \ln P)_{s,\mu} - d\ln T/d\ln P$), and mean molecular weight gradient ($d\ln\mu/d\ln P =: \nabla_\mu$) define the positive directions along the ordinate and abscissa, respectively. The Ledoux-criterion $\nabla = \nabla_{\rm L}$, with $\nabla_{\rm L} = \nabla_{\rm ad} + \frac{\varphi}{\delta}\nabla_\mu$, separates the region of instability with a growth rate of the order of the dynamical time scale (dark gray) from the rest of the diagram. The angle of the line $\nabla = \nabla_{\rm L}$ is arbitrarily set in the plot. Light gray shading implies a growth of the instability on the thermal time scale, white indicates stability. In the above expressions, s stands for entropy, μ for the mean molecular weight, and $\varphi = (\partial \ln\rho/\partial\ln\mu)_{P,T}$ and $\delta = -(\partial\ln\rho/\partial\ln T)_{P,\mu}$.

siderably affect the evolution of massive stars (Maeder 1987, Langer 1991a, Fliegner et al. 1996, Maeder & Meynet 1996, Meynet & Maeder 1997, Langer et al. 1997ab, Schulte-Ladbeck 1997, 1998). In rotating stars, a number of additional instabilities can occur. *Finite rotation* can lead to a global thermal imbalance in the stellar interior, which induces large scale flows, so called meridional circulations (Eddington 1925). Furthermore, the stabilizing/destabilizing action of a third parameter needs to be considered, i.e. the specific angular momentum. *Differential rotation* occurs in all stars, with the possibility of the occurrence of destabilizing angular momentum stratifications and corresponding mixing of chemical elements and angular momentum (cf. Endal & Sofia 1978, Zahn 1983). Of relevance for massive stars are the shear instability (cf. Maeder 1997), the baroclinic instability (Zahn 1983, Spruit & Knobloch 1984), and the Solberg-Høiland and Goldreich-Schubert-Fricke instabilities (cf. Korycansky 1991).

In principle, the coupling of magnetic fields in the stellar interior with the other stabilizing or destabilizing factors needs to be considered. However, we do not even know what the typical field strength in massive stars may be. Thus the estimates about the effects of magnetic fields have to remain largely speculative (cf. Spruit 1998).

2. Evolution of the internal structure of massive stars

We will, in the following, concentrate on models of rotating massive stars. For recent compilations of non-rotating models see, e.g., Langer (1991b), Schaller et al. (1992), Bressan et al. (1993), Langer et al. (1994), Meynet et al. (1994), Stothers & Chin (1996).

2.1. CORE HYDROGEN BURNING: EVIDENCE FROM BORON ABUNDANCES

Massive stars are rapid rotators. Equatorial rotation velocities span the range $v_{\rm rot} = 100 - 400\,{\rm km\,s^{-1}}$, with B stars rotating closest to their break-up speed $v_{\rm crit}$, and values of $v_{\rm rot}/v_{\rm crit} = \omega_{\rm rot}/\omega_{\rm crit} = 0.5$ frequently observed for O stars (Fukuda 1982, Penny 1996, Howarth et al. 1997). During the last decade, many observations have revealed unusual surface abundances that may require additional internal mixing (beyond that of simple convection) for their explanation.

OBN stars have been found to be nitrogen enriched and carbon depleted (Schönberner et al. 1988). It is suspected that even spectroscopically normal OB supergiants are nitrogen-rich, and that only the rare carbon-strong OBC stars show unaltered abundances (Walborn 1988). The SN 1987A progenitor showed evidence of CNO processing (Fransson et al. 1989). A considerable fraction of main sequence B stars was found to be nitrogen enriched by Gies and Lambert (1992), and B (Lennon 1994) and A supergiants (Venn 1996) were also found to be N-enriched, with abundances unlike those expected from dredge up as a red supergiant. And finally, Wolf-Rayet stars of the mixed type WN/C show, simultaneously, the products of hydrogen and helium burning at their surface (Langer 1991c, Crowther et al. 1995).

In contrast to helium and CNO, the light elements are destroyed relatively close to the stellar surface. For both stable boron isotopes, ^{10}B and ^{11}B, the life time against proton capture, the dominant destruction mechanism, is equal to the main sequence life time of a $10\,M_\odot$ star ($\sim 10^7\,$yr) at a temperature of roughly $7\,10^6\,$K. This temperature occurs sufficiently deep inside the stellar envelope (i.e. roughly $1\,M_\odot$ below the surface; cf. Fig. 2) that its surface abundance can not be altered due to mass loss alone on the main sequence in the B star regime. Thus, the boron abundance in B stars is a critical test of mixing processes in the upper stellar envelope, while CNO and helium abundances additionally trace the mixing in deeper layers.

For main sequence secondary stars in massive close binary systems, a strong boron depletion must also be expected due to the transfer of nuclear processed matter; however, a very noticeable CNO-signature is always present in this case (cf. e.g. De Greve & de Loore, 1992). Therefore, the existence of boron depleted stars with a roughly normal nitrogen abundance would be a clear indication of rotational mixing.

Fig. 3 shows the stellar evolution tracks of non-rotating models of 10 and 15 $M_\odot$, and of a moderately ($v_{\rm eq} \simeq 280$ km/s at the ZAMS) and a rapidly rotating ($v_{\rm eq} \simeq 400$ km/s) $10\,M_\odot$ star in the HR diagram. The models have been computed for a composition of (X,Y,Z)=(0.70,0.28,0.02), with up-to-date microphysics input, and including the effects of rotation on the stellar structure and on angular momentum and chemical element transport (cf. Fliegner et al. 1996). The dependence of the stellar tracks on the rotation rate, mostly produced by the fact that faster rotating stars obtain larger helium cores due to more efficient mixing of hydrogen into the

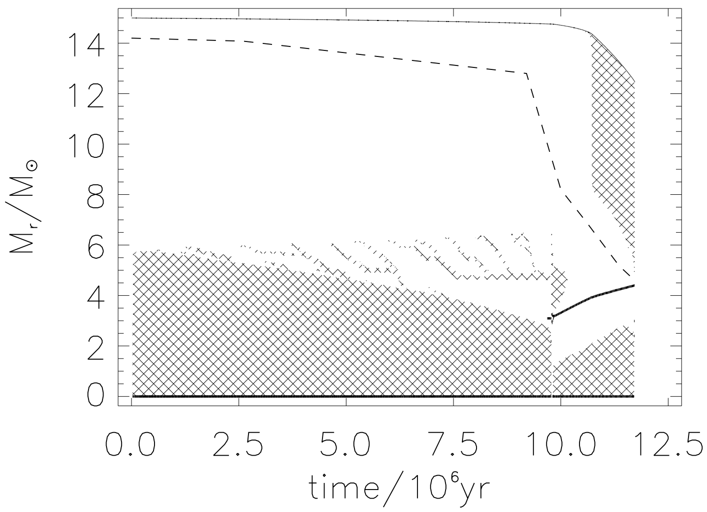

Figure 2. Internal structure of a non-rotating $15\,M_\odot$ star during core hydrogen and helium burning. The solid line on top indicates the total mass of the star as function of time. Hatched areas designate convectively unstable mass zones in the star. The full drawn line at $M_r \simeq 4\,M_\odot$ and $t \gtrsim 10^7$ yr designates the location of the H-burning shell during core helium burning. The dashed line indicates the threshold temperature for the destruction of both stable boron isotopes ^{10}B and ^{11}B of $\sim 7\,10^6$ K, defined by the boron life time being equal to the stellar life time (cf. Fliegner, Langer and Venn, 1996).

core (cf. Langer 1992), has the following consequence. Assuming that stars are born with a distribution of initial rotation rates, there is no clear trend of changes in surface composition due to rotational mixing as a function of the proximity to the zero age main sequence. For example, a non- or slowly rotating star of $15\,M_\odot$, which keeps its initial surface abundances during the main sequence evolution, leads to the same point in the HR diagram as a rapidly rotating $10\,M_\odot$ star which has changed surface abundances. This may explain the lack of a correlation of the N-overabundance with stellar age found by Gies & Lambert (1992).

However, due to the different sampling depths of boron and (e.g.) nitrogen, the models predict a distinct evolution in the boron-depletion vs. nitrogen-enhancement. The boron vs. nitrogen predictions are remarkably similar for models of different masses and rotation rates (see Fig. 4). This is because the evolution proceeds through three different stages of surface abundances: i) An initial phase of unaltered abundances, which lasts roughly $1.5\,10^6$ yr. ii) Boron depletion occurs at the stellar surface without a change in nitrogen, since boron survives in only the outermost $1\,M_\odot$ and nitrogen is synthesized at much deeper layers. iii) After another time span of about $7\,10^6$ yr, nitrogen starts to be enriched with only a small additional boron depletion.

Despite the fact that the average initial abundances of boron and nitrogen for Galactic B stars are not very well known, the agreement of the theoretical B vs. N correlation with the observed values derived by Venn et al. (1996) and Gies & Lambert (1992) is remarkable. The observed abundance pattern has the following properties (Fig. 4):

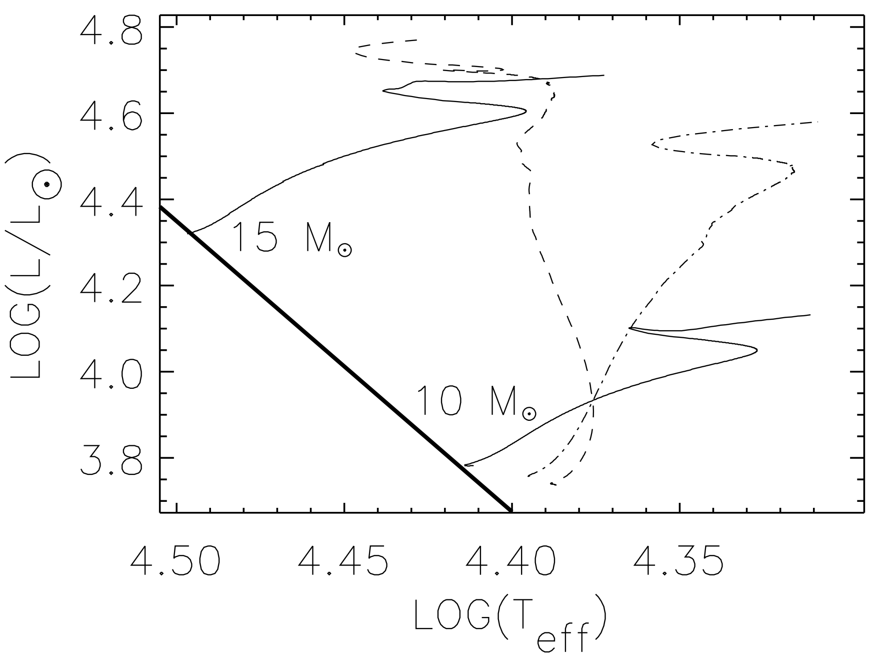

Figure 3. Evolutionary tracks of three $10\,M_\odot$ stars with different initial equatorial rotation velocities ($v_{\rm eq} = 0$, 280, and 400 km/s; solid, dash-dotted, and dashed lines, respectively) during the core hydrogen burning phase. The track of a non-rotating $15\,M_\odot$ star is also shown. The thick solid line marks the ZAMS position of non-rotating stars (from Fliegner, Langer and Venn, 1996).

(1) Main sequence B stars appear to be boron deficient compared to the solar system.

(2) A considerable spread in the boron abundances of very similar main sequence B stars indicates that boron depletion occurs during the main sequence evolution.

(3) A large fraction of main sequence B stars are not strongly enriched in nitrogen.

(4) Another fraction of main sequence B stars are N-enriched.

All four properties are consistent with models of rotating massive main sequence stars, and thus add to the growing list of evidence in favor of rotational mixing. Moreover, the first listed property appears inconsistent with competing massive close binary models in a statistical sense, and the first and the third points together are directly inconsistent with those models, but specifically support the idea of rotational mixing.

In summary, boron abundances appear to be an extremely important diagnostic for the evolution of B stars and cooler luminous stars since rotational mixing on the main sequence deeply affects the post-main sequence evolution. Therefore, a comprehensive study of this element with highest quality data (HST GHRS) for hot stars is highly desirable. This, as well as the analysis of boron in supergiants (cf. Venn et al. 1996) may allow us to considerably reduce persisting uncertainties in the theory of rotational mixing, which is not only fundamental for studying stars

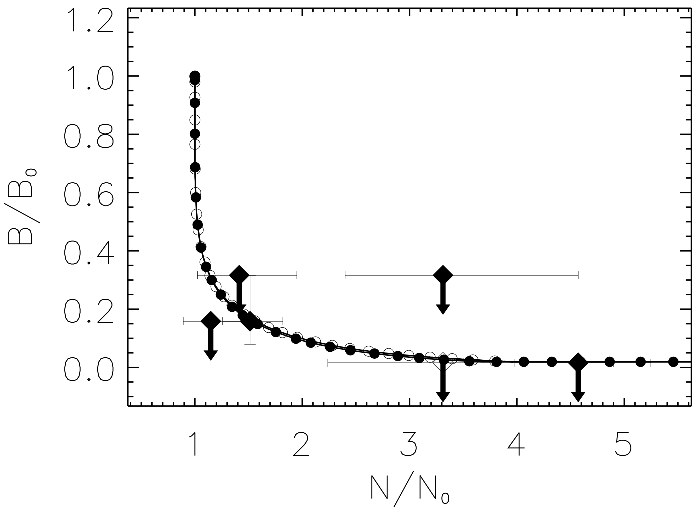

Figure 4. Boron depletion versus nitrogen enrichment for rotating stars of 10 $M_\odot$ during the main sequence evolution (cf. Fig. 3). Open circles correspond to the moderately, filled circles to the fast rotating model. Two neighboring symbols on each line indicate a constant distance in time of 10^6 yr. Diamonds indicate the location of the five B main sequence stars (filled symbols) and one B giant (open symbol) of Venn et al.'s (1996) sample. Arrows designate upper limits (from Fliegner, Langer and Venn, 1996).

within the mass range considered here, but which is also required for a thorough understanding of more massive stars (Maeder 1987, Talon et al. 1997, Heger et al. 1997, 1998).

2.2. BEYOND CORE HYDROGEN BURNING

Fig. 5 displays a set of tracks of rotating and non-rotating stars in the HR diagram, which cover the evolution from the zero age main sequence to the pre-supernova stage (Heger et al. 1998). A major result of these calculations is that the effect of transport of chemical species and angular momentum beyond core hydrogen exhaustion appears to be limited (cf. also Endal & Sofia 1978). The main reason is that strong entropy and mean molecular weight gradients at the location of nuclear shell sources inhibit any efficient mixing. This means that one may not generally expect significant effects on the chemical yields of isotopes synthesized in the post main sequence burning phases. However, as the angular momentum is conserved inside the core, the structure of the star prior to the iron core collapse and the supernova explosion may be strongly affected by rotation (cf. Sect. 2.3).

2.2.1. *Angular momentum transport in contracting convective envelopes*

There are, anyway, two remarkable aspects of rotationally induced transport during the post main sequence evolution of massive stars. The first concerns the transport of angular momentum in the envelope of red supergiants which undergo a blue loop during their core helium burning stage. In order to understand how convective angular momentum transport spins the star up before and during the blue loop, let

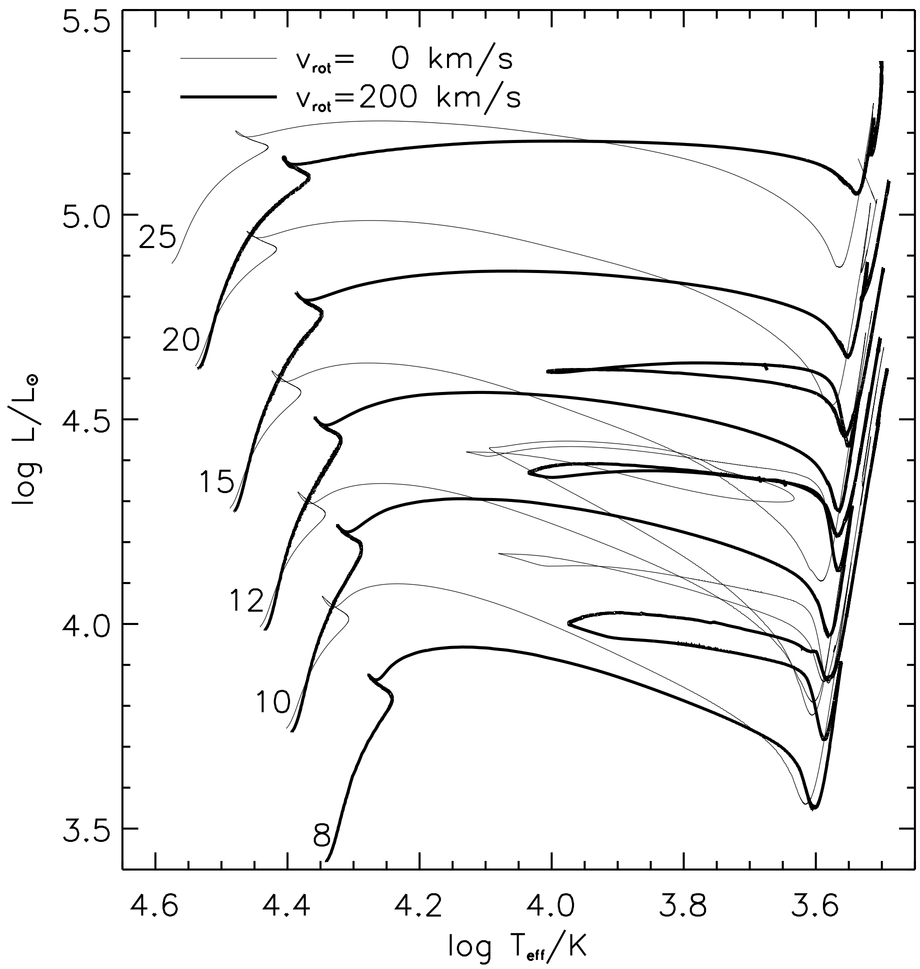

Figure 5. Evolutionary tracks for rotating (thick lines) and non-rotating (thin lines) stars in the mass range 8...25 $M_\odot$ from the ZAMS to the pre-supernova stage (from Heger, Woosley and Langer, 1998). The tracks are labeled with the initial masses (in $M_\odot$).

us first consider the case of mass loss from a rigidly rotating (and non-magnetic) star (Fig. 6, left panel).

The spin-down of mass losing rigidly rotating envelopes can be understood by breaking up the continuous mass and angular momentum loss into three discrete steps; cf. Langer 1998), neglecting secular changes of the stellar structure. Starting from a rigidly rotating envelope extending from R_c to R_0 (A1), the outer part of the convective envelope located between R_1 and R_0 is removed by stellar mass loss within the time interval Δt (A1 $\rightarrow$ A2). In the second step, for which we assume local angular momentum conservation, the envelope re-expands to roughly its original size (A2 $\rightarrow$ A3). This results in a slow-down of the surface rotation and, as the layers deep inside the envelope expand less, differential rotation below (A3). In the third step, rigid rotation is re-established by an upward transport of angular momentum (A3 $\rightarrow$ A4). As this implies an averaging of the angular velocity, it is clear from Fig 6 (A4) that now the whole envelope rotates slower than at the beginning of step 1. Obviously, the redistribution of angular momentum towards

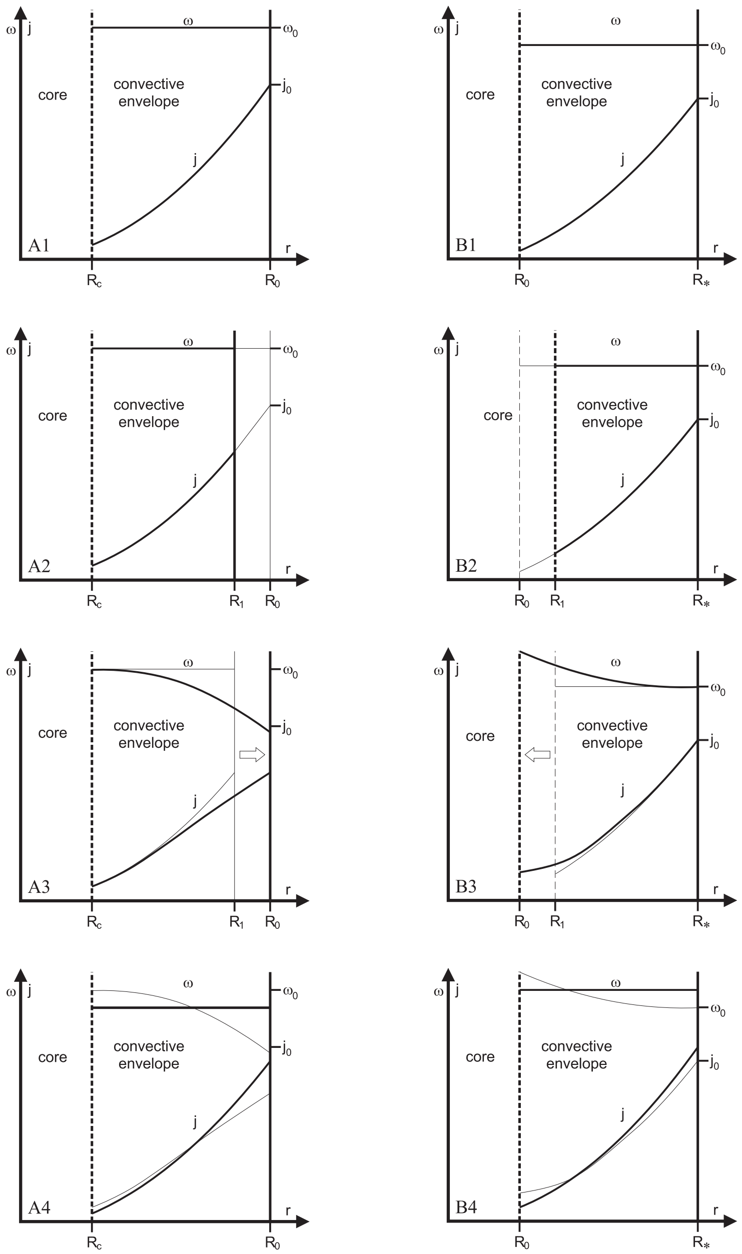

Figure 6. Mass loss from a rigidly rotating stellar envelope from the surface (case A: left panels) and through its lower boundary (case B: right panels), after Heger & Langer (1998). The continuous process is split up into three steps. First (panels $1 \rightarrow 2$), mass gets lost from the envelope, secondly, the envelope restores its original (inner or outer) radius R_0 (panels $2 \rightarrow 3$) by expansion, and third (panels $3 \rightarrow 4$) the specific angular momentum j is redistributed such that rigid rotation (i.e. $\omega(r) = \text{const.}$) is restored. This leads to spin-down (spin-up) and decrease (increase) of the mean specific angular momentum for the case of mass loss through the upper (lower) boundary of the rigidly rotating stellar envelope. Thin lines show the state of the preceding step.

the stellar surface leads to an increase of the angular momentum loss rate.

The spin-up of convective envelopes which decrease in mass due to an outflow through their *lower* boundary — which happens in red supergiants prior to a blue loop (cf. below) — is understood in a similar way. Again we want to split up this process into three discrete steps (see sequence B on the right hand side of Fig 6).

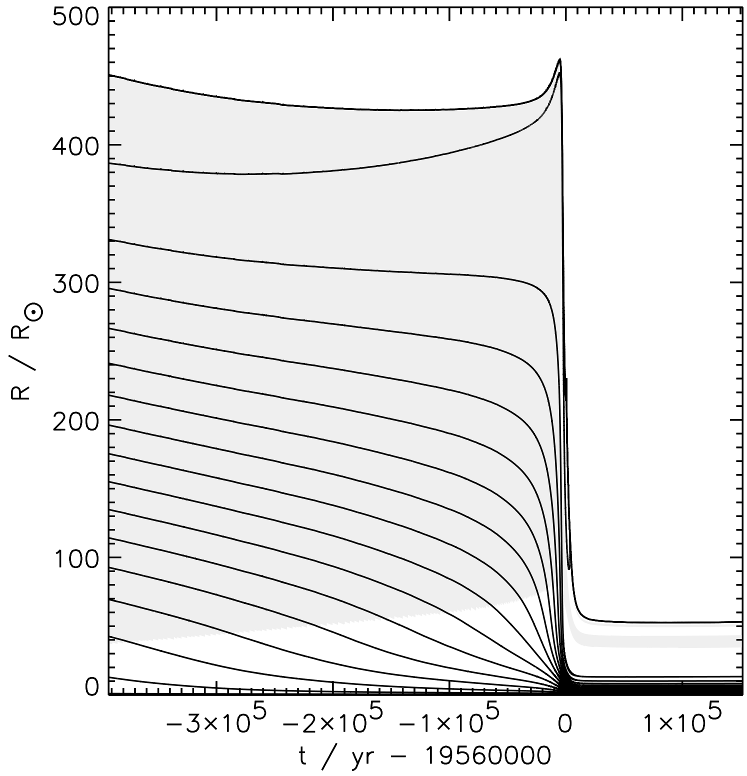

Figure 7. Evolution of the radii of different mass shells as a function of time for a period including the transition from the red to the blue supergiant stage of a rotating 12 $M_\odot$ model (from Heger & Langer 1998; cf. also Fig. 5). $t = 0$ is defined as in Fig. 16 below; it corresponds roughly to the time of the red-blue transition. Except for the uppermost solid line, which corresponds to the surface of the star, the lines trace Lagrangian mass coordinates. The mass difference between the lines is 0.5 $M_\odot$. Shading indicates convection.

Starting from a rigidly rotating envelope extending from R_0 to $R_\star$ (B1), the inner part of the convective envelope, located between R_0 and R_1, becomes radiative within some time Δt (B2). Then the envelope re-expands to its original size. As local angular momentum conservation is assumed in this step, it results in a spin-up of most of the convective envelope, which is weaker for the layers farther out. The outcome is a differentially rotating envelope which spins fastest at its bottom (B3). Since the envelope has to go back to rigid rotation, angular momentum is transported upward in the next step until this is achieved (B4). We end up with higher specific angular momentum in the whole convective envelope compared to the initial configuration.

As can be seen in Fig 7, during the evolution of a red supergiant towards the blue part of the HR diagram the radial extent of the convective envelope remains about fixed while mass shells drop out of the convective region. If one imagines the convective envelope to consist of moving mass elements or blobs, the spin-up process can also be understood as follows. A blob, starting somewhere in the convective region will, as it approaches the lower edge of the convective envelope, decrease its specific moment of inertia and therefore has to lose angular momentum in order to remain in solid body rotation with the whole convective region. Angular momentum has to be transferred to rising blobs such that also they remain in solid body rotation. Mass elements leaving the convective envelope thus only remove small amounts of angular momentum from the convective region. Therefore, the average specific angular momentum of the remaining convective envelope will increase and thus it spins up dramatically. The observable consequences of this spin-up are discussed in Sect. 3.3.

2.2.2. *Chemical mixing through shell sources*

While during the spin-up process discussed above angular momentum is not transported through chemical gradients or discontinuities, we want to mention, as a second example of important rotationally induced mixing after core hydrogen exhaustion, the possibility of chemical mixing in the case of extinct shell sources.

Just as rotation alters the composition of the H-rich envelope of massive main sequence stars, it can also mix the ashes of advanced burning stages with the radiative mantles above the burning cores, though this process is limited by the progressively shorter evolutionary time scales. Qualitatively new nucleosynthesis channels are opened in the situation where this mixing can transport the products of one burning phase to the site of a neighboring burning stage. This remains difficult, as neighboring burning stages are frequently separated by large entropy differences. However, we have identified two possibilities: **a)** When — during late burning stages — the H-burning shell becomes extinct, protons can be transported into the helium burning shell source (Fig. 8). **b)** In stars of very low metallicity, the entropy difference between the H- and He-burning shell is small. In a $20\,M_{\odot}$ star of $Z = 10^{-3}Z_{\odot}$, we find ^{12}C to be injected into the H-burning shell and protons into the He-burning shell.

The injection of protons into helium burning results in a large rapid release of neutrons via $^{12}\mathrm{C}(p,\gamma)^{13}\mathrm{N}(\beta^{+}\nu)^{13}\mathrm{C}(\alpha,n)$. We are presently exploring the consequences but it is already clear that if a considerable amount of protons can be injected into the He-shells of stars of $\sim 10\,M_{\odot}$, this site may become again interesting as r-process source either before or during the supernova explosion (Cowan et al. 1983). In any case, the rather mild s-process usually associated with massive stars will change dramatically. Furthermore, a similar mechanism might act in thermally pulsating AGB stars where the periodic fading of the H-burning shell results in a periodic reduction of the entropy barrier between the H- and He-burning shell. I.e., rotational mixing is a candidate for producing the ^{13}C-pocket needed to operate the main component s-process in ABG stars.

The injection of ^{12}C into the H-burning shell on the other hand results in the production of primary ^{14}N. About $0.01\,M_{\odot}$ of ^{14}N are synthesized in this way in our rotating metal-poor ($10^{-3}\,Z_{\odot}$) $20\,M_{\odot}$ star. This may be sufficient to account for the nitrogen observed in the most metal poor stars (Laird 1985, Carbon et al. 1987). The investigation of the mass and metallicity dependence of this process needs further studies of rotating low-metallicity stars.

2.3. PRE-SUPERNOVA STRUCTURE

As outlined in Section 2.1, one of the principle effect of rotation is to increase the mass of the helium core. An increased core mass has consequences for all subsequent burning stages, as the core mass determines which temperatures and densities are achieved in the course of stellar evolution. Since the cores contain the ashes of hydrostatic nuclear burning stages, the corresponding chemical yields of massive

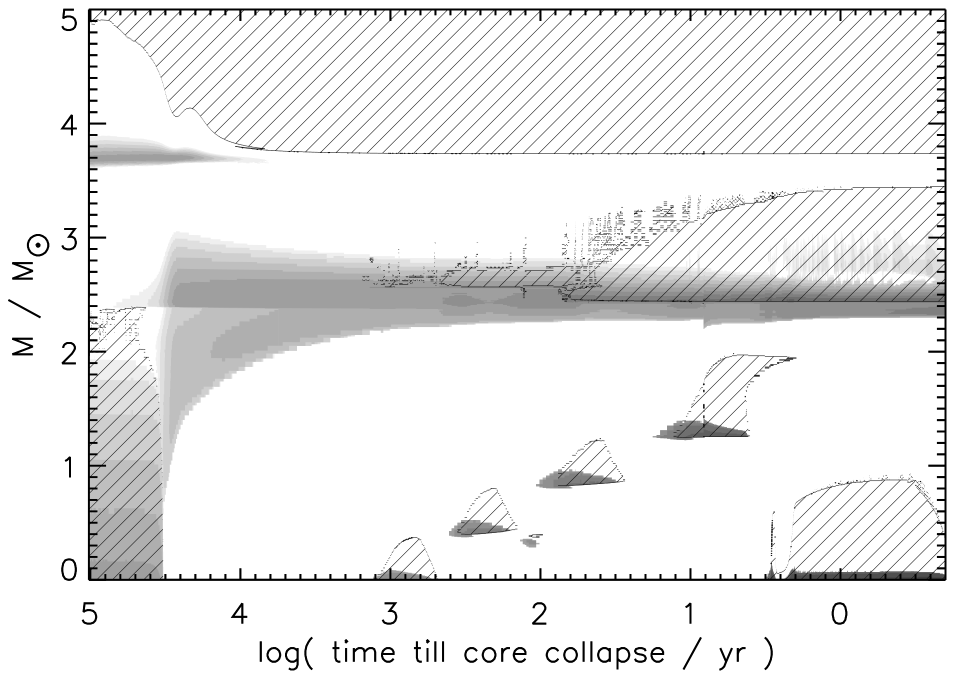

Figure 8. Structure of the inner 5 $M_\odot$ of a rotating star with an initial mass of 12 $M_\odot$, an initial equatorial rotation velocity of 200 $\mathrm{km\,s^{-1}}$ and solar metallicity, from core-He exhaustion through core-O burning (from Heger, priv. communication; cf. also Langer et al. 1997b, and Heger, Woosley and Langer 1998). The abscissa is the logarithm of the time left until core collapse, and the ordinate is the mass enclosed in successive equipotential surfaces (cf. text). Dark shading indicates net positive nuclear energy generation, with the grey scale extending from $10^{-1}\,\mathrm{erg\,g^{-1}\,s^{-1}}$ (lightest grey) to $10^{12}\,\mathrm{erg\,g^{-1}\,s^{-1}}$ (darkest shading). Hatched regions are convectively unstable. The final stellar mass is 10.4 $M_\odot$, and the convective H-rich envelope extends down to $M \simeq 3.8\,M_\odot$. The He-burning shell is located at $M \simeq 2.5\,M_\odot$. During the last several 100 years the combined action of rotational mixing processes and the extending convective shell above the He-shell source episodically sweeps protons into the helium burning region, which leads to a flickering of the shell source and associated neutron production events.

stars — e.g. that of oxygen — are increased by rotation (cf. Langer et al. 1997b). However, while this effect can become of the order of tens of percent, also qualitative changes can be caused by increased core masses. An example is shown in Fig. 9, which compares the evolution of a non-rotating and a rotating 10 $M_\odot$ star in the $\rho_c - T_c$-diagram. While the latter evolves straight through all nuclear burning stages to become a Type II supernova, the non-rotating star ignites carbon in a degenerate core off-center and then cools and may become an ONeMg white dwarf (cf. Ritossa et al. 1996).

As mentioned above (Sect. 2.2), active nuclear shell sources appear to inhibit the transport of chemical elements and of angular momentum. Heger et al. (1998) found that after core hydrogen exhaustion — i.e. after the ignition of the first nuclear shell source — the specific angular momentum j of the core remains roughly constant (cf. Table 1). This has the consequence that the collapsing iron core (assuming local angular momentum conservation during the collapse) will reach critical rotation. The calculations of Heger et al. (1998) are the first of its kind, and they should still be considered as preliminary. Major uncertainties arise due the poorly known influence of molecular weight gradients on the shear instability (cf. Maeder 1995,

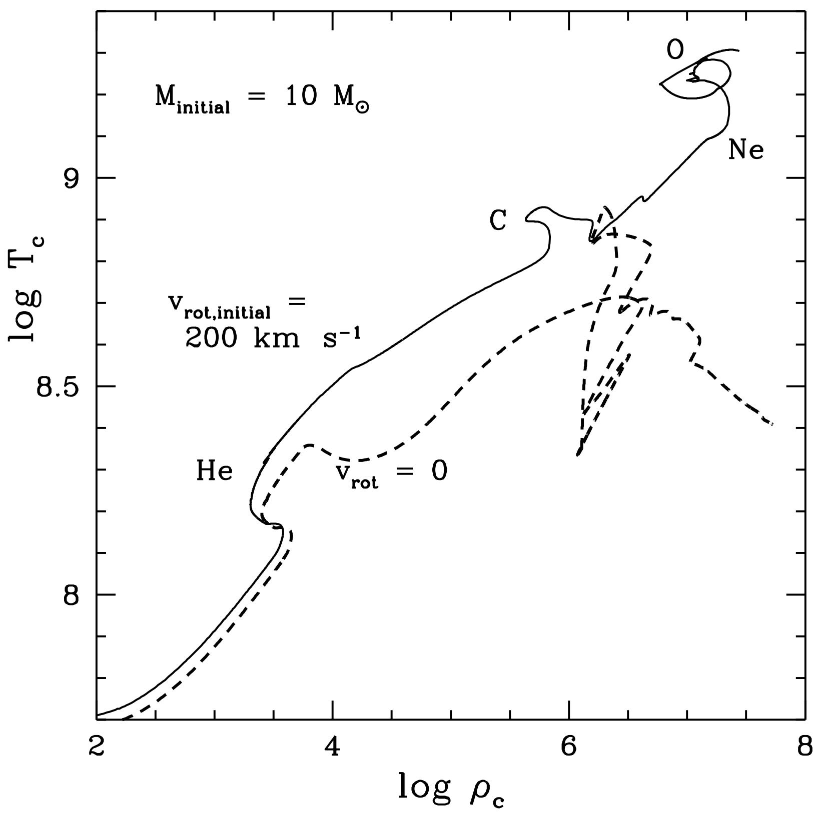

Figure 9. Evolutionary tracks of a rotating (solid line) and a non-rotating (dashed line) 10 $M_{\odot}$ star in the $\log \rho_c - \log T_c$–diagram (from Langer et al 1997b). The various core burning stages are indicated along the track of the rotating model.

TABLE 1. Properties of a 20 $M_{\odot}$ star at the mass coordinate $M_r = 1.7\,M_{\odot}$ (the mass of the iron core) at various times during the evolution (cf. Heger et al. 1998).

evol. stage	j cm^2/s	r cm	ρ g/cm^3	ρ_c g/cm^3	ω s^{-1}	ω/ω_c
ZAMS	$1.1\,10^{17}$	$5.8\,10^{10}$	3.7	4.8	$5\,10^{-5}$	0.046
H-exh.	$2\,10^{16}$	$4.3\,10^{10}$	8.2	12.5	$1.6\,10^{-5}$	0.010
He-exh.	$1.3\,10^{16}$	$7.2\,10^{9}$	1650	$3\,10^{3}$	$3.8\,10^{-4}$	0.015
pre-collapse	$1.2\,10^{16}$	$2.2\,10^{8}$	$1\,10^{9}$	$4\,10^{9}$	0.37	0.08
n-star	(10^{16})	$1.2\,10^{6}$	—	$4\,10^{14}$	10^{4}	0.91

1997) and our ignorance of the effect of magnetic fields in the stellar interior on the transport of chemicals and angular momentum (cf. Spruit 1998). However, if confirmed, their results have strong implications for Type II and Ib/c supernovae and the resulting neutron stars (cf. Langer et al. 1997b), in particular for the core

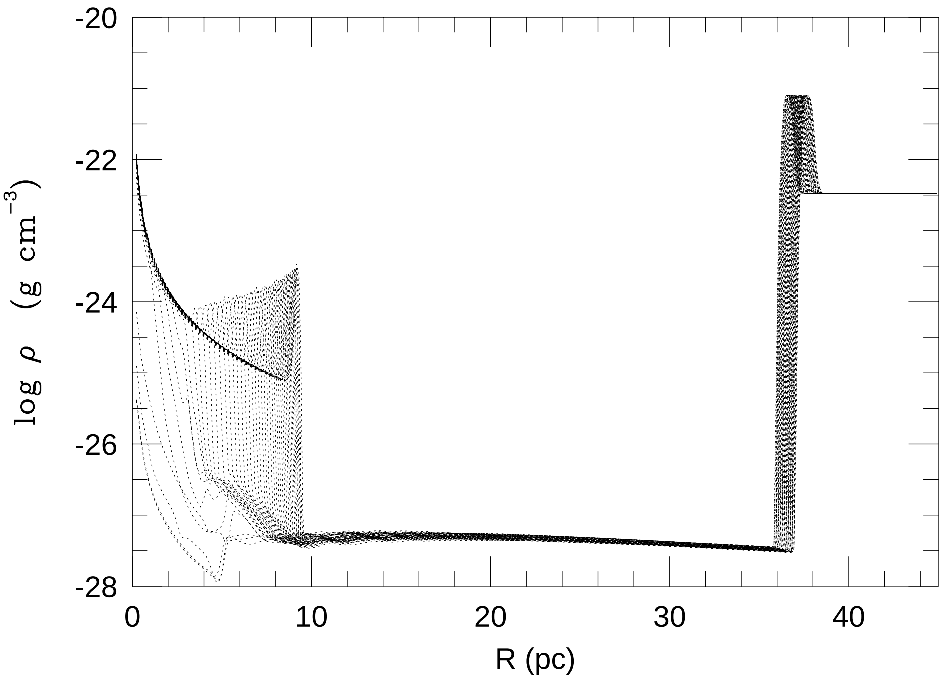

Figure 10. Logarithm of the density as function of radius for various times, starting from the end of the main sequence phase (lowest profile) and covering the whole red supergiant phase of a 35 $M_\odot$ star (from García-Segura, Langer and Mac Low, 1996b). The time difference between profiles is 4000 yr. The shell swept up from the main sequence wind at $\sim$ 36 pc remains almost constant during this time, while in the inner 10 pc the development of the RSG shell inside the MS bubble can be seen. This plot corresponds to our calculations assuming a *fast* RSG wind (75 km s^{-1}). The largest RSG wind shell radius obtained in the case of a *slow* RSG wind (15 km s^{-1}) is only 3 pc.

collapse supernova mechanism (e.g., Yamada & Sato 1994, Aksenov et al. 1997).

3. Evolution of the circumstellar matter around massive stars

The stellar winds, radiation fields, and final supernova explosions of massive stars heat the surrounding gas, chemically enrich it, and sweep it into large shells, possibly even inducing star formation. By studying the interaction of the ejected gas with the interstellar medium (ISM), we can learn about the energy balance of the ISM and the chemical enrichment of the Galaxy. To understand these dynamical processes, we must understand the structure and evolution of massive stars, and their atmospheres and winds.

For non-rotating stars, the hydrodynamic evolution of the circumstellar medium has been computed self-consistently with the evolution of the central stars for the two initial masses 60 $M_\odot$ — where the evolution proceeds as O-star $\rightarrow$ Luminous Blue Variable $\rightarrow$ Wolf-Rayet star (García-Segura et al. 1996a) — and 35 $M_\odot$, which evolves as O-star $\rightarrow$ red supergiant $\rightarrow$ Wolf-Rayet star (García-Segura et al. 1996b; see also García-Segura & Mac Low 1995ab). It has been shown that massive stars

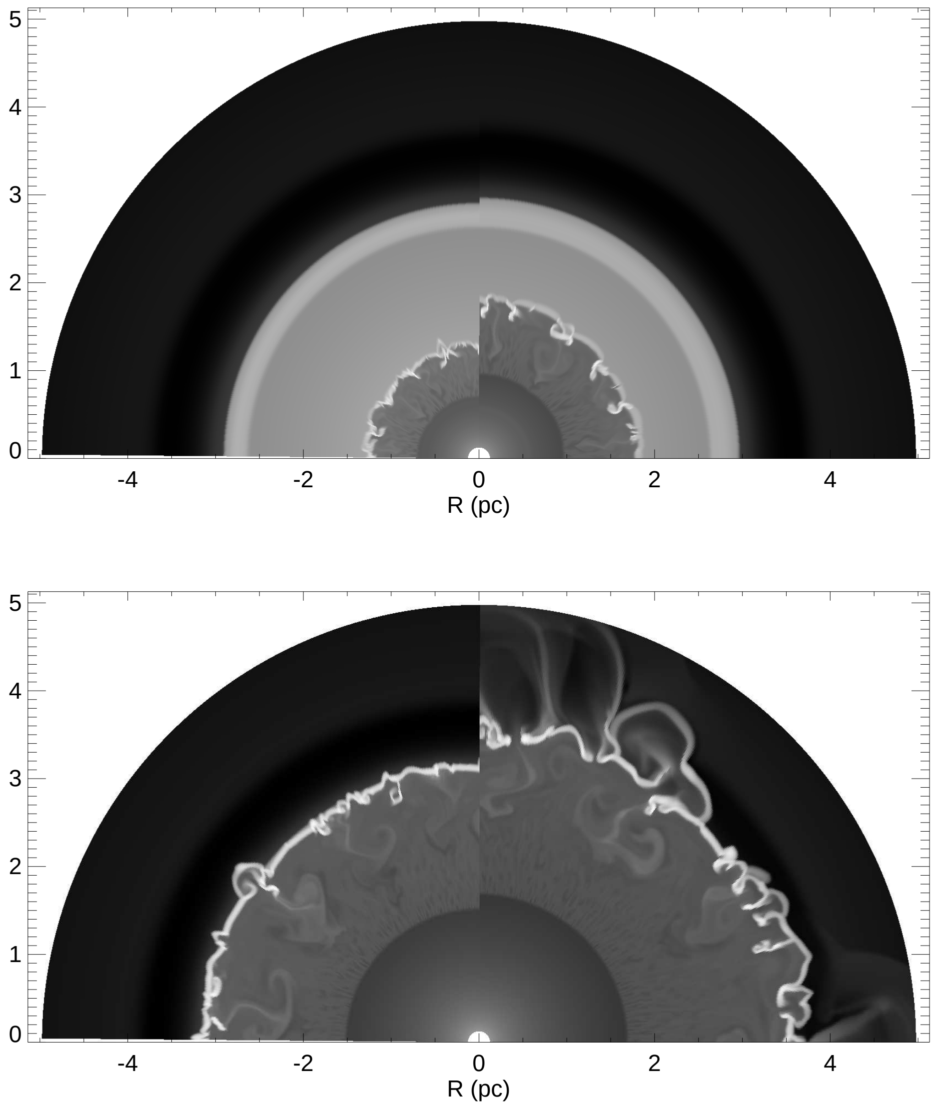

Figure 11. Grey scale plot of the logarithm of the gas density (in g cm^{-3}) corresponding to the early Wolf-Rayet phase of the 35 $M_{\odot}$ stellar model sequence (cf. Fig. 10; from García-Segura, Langer and Mac Low, 1996b). A slow red supergiant wind velocity (15 km s^{-1}) has been assumed for this calculations. The time difference between two successive 90° plots is 2490 yr. The gray scale goes from min=-27.0 (black) to max=-20.8 (white), except for the first panel, where the max=-20.6.

live in a hot bubble created by the interaction of the O star wind with the surrounding interstellar medium (cf. Weaver et al. 1977). Successive slow and fast winds, or slow winds blown into the hot bubble, lead to the creation of circumstellar shells which are spherically symmetric for spherical winds (cf. Fig. 10, for the red supergiant stage of the 35 $M_{\odot}$ calculation) but often fragment due to hydrodynamic instabilities (Fig. 11).

The circumstellar matter around many stars shows a remarkable axial symmetry. Famous examples comprise Supernova 1987A (Plait et al. 1995; Burrows et al.

1995), the Homunculus nebula around η Carina and other nebulae around so called Luminous Blue Variables (Nota et al. 1995), and many planetary nebulae (Schwarz et al. 1992). A less spectacular example are B[e] stars, blue supergiants showing properties which might be well explained by a circumstellar disk (Gummersbach et al. 1995; Zickgraf et al. 1996ab). Many of these axisymmetric structures have been explained in terms of interacting winds of rotating stars (cf. Martin & Arnett 1995; Langer et al. 1998; García-Segura et al. 1998). However, for that the stars need to rotate with a considerable fraction of the break-up rate (Ignace et al. 1996; Owocki et al. 1996). In the following we investigate during which phases massive stars can reach critical rotation in their surface layers.

3.1. THE Ω-LIMIT

In a hydrostatic rotating star, the momentum equation has to include the centrifugal acceleration $a'_{\rm cen}(r,\theta) = a_{\rm cen}(r)\cos(\theta)$, where θ is the latitudal coordinate. To obtain a stability criterion, we follow Langer (1997) and only evaluate the momentum equation at the stellar surface, where density inversions and convective flux contributions are negligible. Furthermore, we concentrate on the equatorial plane, since there the destabilizing centrifugal term is largest. Defining $v^2_{\rm rot}/R := a_{\rm cen}(R, 0^\circ)$, we are left with a momentum balance as $a_{\rm rad} + g + v^2_{\rm rot}/R = 0$ or $\frac{1}{R}\left(\frac{\kappa L}{4\pi Rc} + \frac{GM}{R} + v^2_{\rm rot}\right) = 0$. We can thus define

$$v^2_{\rm crit} := \frac{GM}{R}(1-\Gamma) \tag{1}$$

and obtain as criterion for instability

$$\Omega := \frac{v_{\rm rot}}{v_{\rm crit}} > 1. \tag{2}$$

It is crucial to realize that for $\Gamma \rightarrow 1$ Eq. (1) gives $v_{\rm crit} \rightarrow 0$. Therefore, if we assume a star to evolve towards the Eddington limit ($\Gamma \rightarrow 1$), no matter what its rotation rate may be, it will arrive at critical rotation well *before* $\Gamma = 1$ is actually reached. Therefore, one may rather speak of the "Ω-limit" instead of the Eddington limit.

As a consequence, the location of the occurrence of the instability in the HR diagram depends on the stellar rotation rate. In contrast to the Eddington limit, the Ω-limit is not — for a fixed metallicity and L/M-relation — a single line in the HR diagram. Furthermore, while the most massive stars may arrive at the Ω-limit independent of their rotation speed, it may happen that two less massive single stars start with the same initial mass and metallicity, but only the faster rotating one arrives at the Ω-limit while the slower one does not and evolves further into the red supergiant region. This scenario might apply to the less luminous LBVs, which do have red supergiant counterparts of equal luminosity.

A second consequence is that the outflow which occurs due to a star hitting the Ω-limit is predicted to be highly bipolar. This is illustrated by a hydrodynamical simulation of the giant eruption of η Car (cf. Sect. 3.3). The fact that virtually all LBV nebulae are highly bipolar (Nota et al. 1995, Schulte-Ladbeck 1997) supports the idea that the Ω-limit is actually involved in the LBV instability.

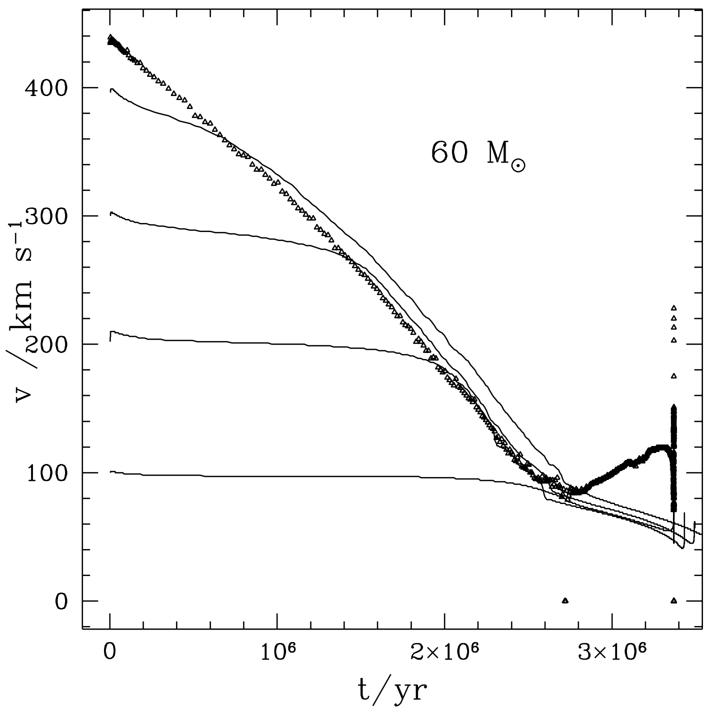

Figure 12. Evolution of the equatorial rotation velocity with time during the core hydrogen burning phase of four 60 $M_{\odot}$ stars with different initial rotation rates (see at $t = 0$). The thick line displays the evolution of the critical rotational velocity for the sequence with an initial rotation velocity of 100 km s^{-1}; it is very similar for the other sequences. The stars are assumed to maintain rigid rotation, and the evaluation of $v_{\rm crit}$ is uncertain. For $v_{\rm rot} \simeq v_{\rm crit}$, the stars evolve at the Ω-limit (cf. Langer 1998).

3.2. CORE HYDROGEN BURNING

Langer (1998) has performed calculations for rigidly rotating core hydrogen burning stars with an initial mass of 60 $M_{\odot}$, initially rotating with different velocities. The assumption of rigid rotation appears to be justified, as the time scale for angular momentum transport in massive main sequence stars is of the order of the thermal time scale (Chaboyer & Zahn 1992, Zahn 1992, 1994, Talon & Zahn 1997). Fig. 12 shows the time evolution of the critical rotational velocity (Eq. 1) and the actual rotational velocity for the computed sequences. The critical rotational velocity (which is roughly the same for all sequences) has a pronounced minimum at roughly $t = 2.6\,10^6$ yr, which corresponds to a stellar effective temperature of about $T_{\rm eff} \simeq$ 36 500 K, around which the iron opacity peak has its maximum effect. We see in Fig. 12 that, as $v_{\rm rot}$ approaches $v_{\rm crit}$ (i.e. $\Omega \to 1$) the rotation rate of the star declines such that the Ω-limit $\Omega = 1$ is never exceeded. This behavior is explained by the coupling of angular momentum and mass loss, which has been explained in Sect. 2.2.1 (cf. Fig.6, left panel).

When the 60 $M_{\odot}$ sequences in Fig. 12 approaches $\Omega = 1$, the mass loss rate is increased (cf. Friend & Abbott 1986). As a consequence, according to the coupling

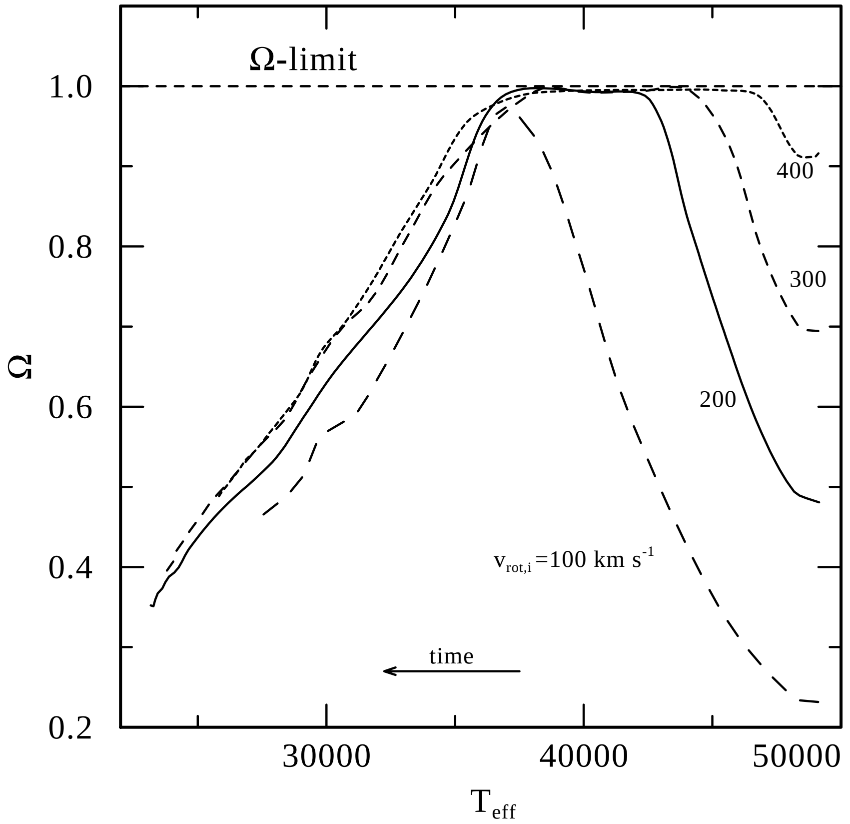

Figure 13. Evolution of the ratio of the rotation rate to the critical rotation rate, Ω, as function of the effective temperature during core hydrogen burning, for $60\,M_\odot$ sequences starting with different equatorial rotational velocities $v_{\rm rot,i}$ (from Langer 1998).

described above, the spin-down rate of the star increases as well. In this situation, i.e. at the Ω-limit, an equilibrium value $\Omega_{\rm eq} < 1$ will establish. It is defined such that if Ω is smaller than this value, mass and angular momentum loss are too small to prevent the star's continuous evolution towards the Ω-limit. If $\Omega > \Omega_{\rm eq}$, the corresponding angular momentum loss is so large that the star evolves away from the Ω-limit, i.e. Ω becomes smaller. In the case of the $60\,M_\odot$ sequences displayed in Fig. 12, it is $\Omega_{\rm eq} \simeq 0.99$.

It is important to realize that the equilibrium mass loss rate at the Ω-limit $\dot{M}_\Omega$ is determined by the condition of a sufficient angular momentum loss to not exceed the Ω-limit. Therefore, for a given critical rotational velocity, the mass loss rate of a rigidly rotating star at the Ω-limit is determined by its density distribution $\rho(r)$ and by its expansion rate due to the internal evolution. Within these assumptions, the mass loss rate does not depend on microscopic properties of the matter as e.g. in the case of the normal hot star winds.

Since the critical rotation velocity evolves almost equally for all considered sequences, the stars leave the Ω-limit at almost the same time and with almost the same rotation rate. However, as they spend different amounts of time at the Ω-limit (cf. Fig. 13), their masses at core hydrogen exhaustion are different, i.e. lower for higher initial rotation velocities (cf. Fig. 14).

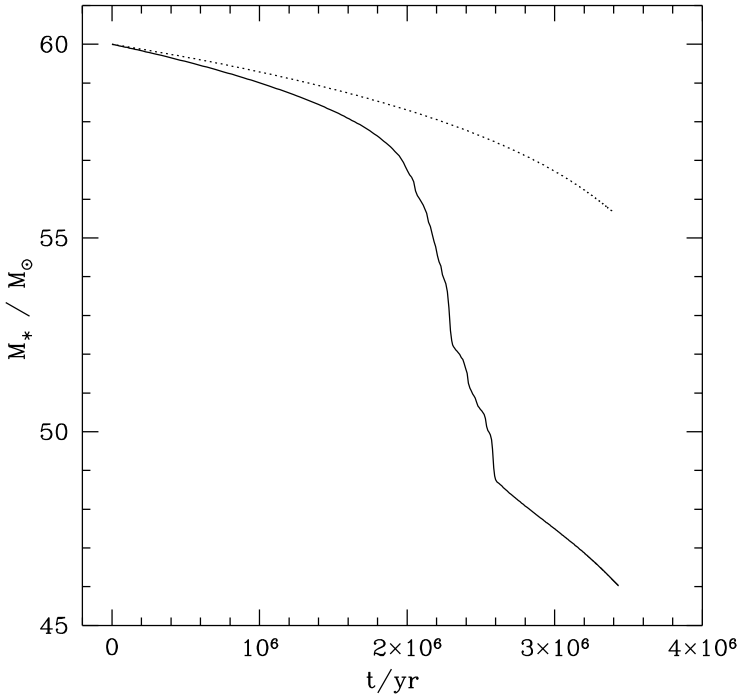

Figure 14. Stellar mass as a function of time for a 60 $M_\odot$ sequence evolving at the Ω-limit (solid line; cf. text), in comparison to the evolution of a 60 $M_\odot$ star without enhancement of the mass loss rate due to rotation (dotted line). The mass loss rates can be read off this figure as the slope of the curves (from Langer 1998).

Since it is also unclear which fraction of the mass lost at the Ω-limit can actually be pushed to infinity by the radiation force, there are several alternatives for the appearance of stars at the Ω-limit. If all the matter is blown away, the star may not look peculiar at first glance. It is important to note that it needs not even to be a rapid rotator (cf. Fig. 12). However, it's mass loss should be strongly enhanced and distinctly non-spherical. The latter might be observable through line profile shapes (cf. Petrenz & Puls 1996, Howarth et al. 1997). In this context, the anomalously high mass loss of some massive O stars in the LMC found by de Koter et al. (1997) may be interesting. The asphericity of the mass loss at the Ω-limit together with its spherical symmetry before and after that phase may result in bipolar circumstellar structures, perhaps like those found around the O6.5 star HD 148937 (Leitherer & Chavarria 1987). As mentioned in Section 3.4, a similarity to B[e] stars may be present if not all the matter is pushed to infinity (cf. also Langer & Heger 1998).

The coupling of mass and angular momentum loss also opens the possibility to deduce average mass loss rates of main sequence stars from the dependence of the mean projected rotational velocity from the effective temperature. However, the observational data, although not inconsistent with the 60 $M_\odot$ models presented by Langer (1998), allows no firm conclusions at present.

3.3. LUMINOUS BLUE VARIABLES

The mass loss rate at the Ω-limit depends on the evolutionary speed of the star in the HR diagram. One can expect values of the order $10^{-5}\ M_{\odot}\ \mathrm{yr}^{-1} \times \tau_{\mathrm{H}}/\tau_{\mathrm{KH}}$ for the expansion phase after core H-exhaustion, when the star hits the Ω-limit again due to the helium opacity peak. Here, τ_{H} is the H-burning time scale — i.e. the expansion time scale on the main sequence — and τ_{KH} the thermal time scale of the star — i.e. its expansion time scale after core hydrogen exhaustion —, such that values of $\dot{M}_{\Omega}$ of the order of $10^{-3} - 10^{-2}\ M_{\odot}\ \mathrm{yr}^{-1}$ can be expected, which is the order of magnitude observed for outbursts of Luminous Blue Variables.

Along this line of thought, García-Segura et al. (1997) and Langer et al. (1998) have performed hydrodynamic calculations for the interaction of three successive winds in order to model the Homunculus nebula around the Luminous Blue Variable η Carinae. They divide the evolution of the circumstellar medium of a star approaching the Ω-limit — i.e., going through an outburst in this case — into three phases. In the first phase, before the star reaches the Ω-limit ($\Omega < 1$), it behaves like a normal supergiant; in particular stellar rotation does not strongly affect its wind, so it has the fast, energetic wind expected of a luminous blue star. In the second phase, reaching the Ω-limit ($\Omega \simeq 1$) has three consequences for the wind: the mass loss rate is much higher than before; the mass flux increases strongly at latitudes close to the equator, where the stellar surface is force-free; and the bulk of the wind is slow since the equatorial escape velocity is almost zero. In the third phase, the outburst is over, the stellar radius has decreased, and the configuration is similar to the first phase. The smaller value of Γ before and after the outburst has two consequences: larger wind velocities due to larger escape velocities *and* smaller values of Ω leading to more spherical winds.

The computation of the hydrodynamic evolution of the circumstellar gas is started at a time of $t = 1840\,\mathrm{yr}$ — the decade of η Car's last major eruption — and continued until $t = 1995\,\mathrm{yr}$. This scenario leads to a characteristic distribution of the circumstellar gas. The initial fast wind blows a stellar wind bubble which forms the background for the subsequent development of the nebula. During outburst, the wind becomes slow and dense, and the stellar rotation concentrates it toward the equatorial plane (Bjorkman & Cassinelli 1993, Ignace et al. 1996). When the final fast wind starts in the center of this nebula, it sweeps up the dense wind from the outburst into a thin, radiatively cooled shell that fragments due to dynamical instabilities (García-Segura et al. 1996a). The shell expands more easily into the lower density wind at the poles, producing a double-lobed structure, as shown in Fig. 15.

This model extends other recent hydrodynamic models for bipolar LBV nebulae (Nota et al. 1995, Frank et al. 1995) by relating the outburst to the properties of evolving massive post-main sequence stars, and by connecting the shape of the nebula directly to the outburst mechanism. Earlier models concluded that a strong equatorial density enhancement must have existed before the outburst occurred. We obtain self-consistently from our model, however, not only the two lobes, including their small-scale structure, but also the equatorial density enhancement, and relate both to the evolutionary state of the star.

In fact, a general mechanism for giant LBV outbursts is needed in order to understand the absence of stars beyond the Humphreys-Davidson limit in the HR diagram (cf. also Pasquali et al. 1997), and the bipolar nature of most LBV nebulae. Therefore, even though bipolar nebulae may also form from interacting binary stars

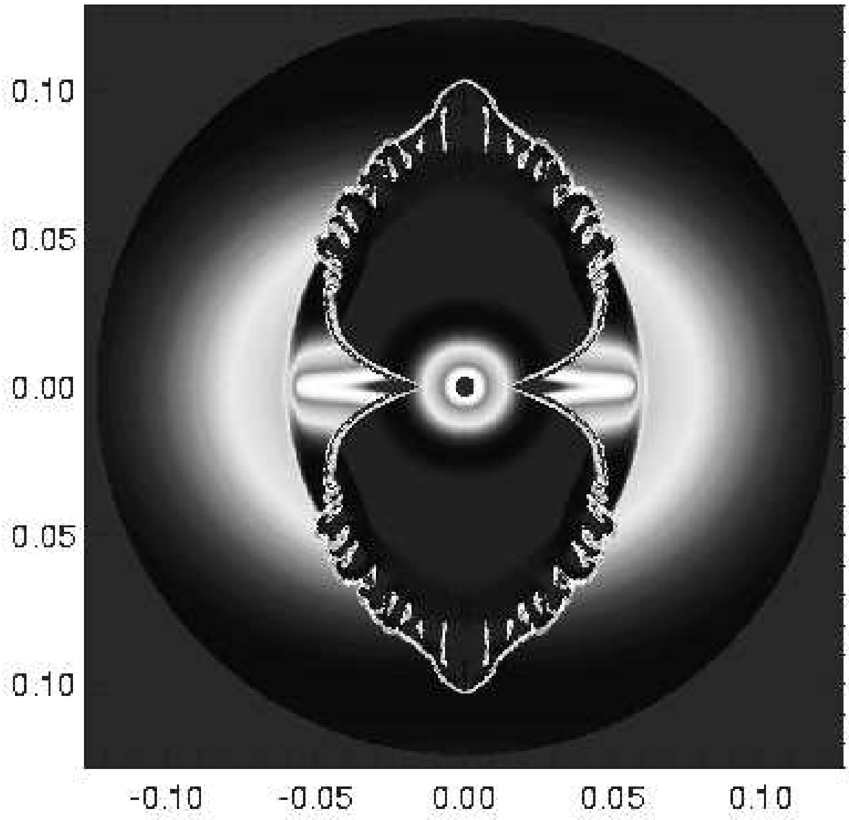

Figure 15. Logarithm of the circumstellar gas density (in g cm^{-3}) in the hydrodynamic model of García-Segura, Langer and Mac Low (1997), and Langer, García-Segura and Mac Low (1998), at $t = 1995$ yr. The density scales from $10^{-21}...10^{-19}$ g cm^{-3}.

(e.g. Han et al. 1995), and binarity has been repeatedly proposed also for η Car (van Genderen et al. 1994, Damineli et al. 1997), it appears useful to continue to pursue single star models. The conjecture that the Homunculus nebula of η Car is a paradigm rather than a freak has recently been supported by its strong similarity to the nebula around the LBV HR Carinae, as found by Weis et al. (1997) and Nota et al. (1997).

3.4. CORE HELIUM BURNING AND BEYOND

As mentioned in Sect. 2.2, stars which evolve from the Hayashi line towards the hotter part of the HR diagram may be spun up significantly. Fig. 16 shows that, for the case of a $12\,M_\odot$ model (cf. Figs. 5 and 7) the star reaches the Ω-limit. The contraction of the star by a factor of ~ 10 (cf. Fig. 7) reduces the specific moment of inertia at the surface by ~ 100 and the angular velocity would be increased by the same factor if specific angular momentum were conserved locally. This would imply an increase of the equatorial rotational velocity by a factor of ~ 10 (cf. Fig. 16, “decoupled”). The true increase in the rotational velocity is one order of magnitude larger, due to the spin-up effect described in Sect. 2.2.1, and it would

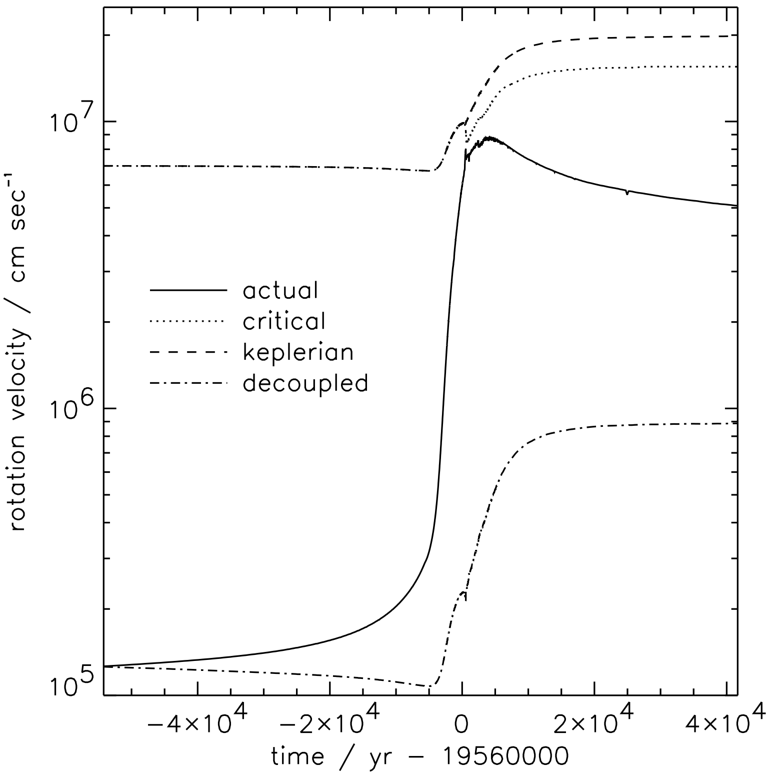

Figure 16. Equatorial rotation velocity as a function of time (solid line) of a 12 $M_\odot$ star during its evolution from the red to the blue supergiant stage (cf. Figs 5 and 7), compared to the Keplerian (dashed line) and the critical (dotted line) rotation rate; the latter two are different by the factor $1-\Gamma$. $t=0$ is defined as in Fig. 7 (see above). During the red supergiant phase it is $\Gamma \ll 1$ and the two lines coincide, while during the blue supergiant phase Γ rises to 0.4. The dash-dotted line shows the evolution of the surface rotation rate if there were no angular momentum transport in the convective envelope (from Heger & Langer 1998).

be even larger if the star would not arrive at the Ω-limit and lose mass and angular momentum at an enhanced rate.

An interesting example where the spin-up mechanism described almost certainly occurred is the progenitor of SN 1987A. In fact, the SN 1987A progenitor is the only star of which we are reasonably sure that it performed a blue loop, in this case after core helium exhaustion (cf. Arnett et al. 1989, Langer et al. 1989)

The structures observed around SN 1987A seem to be rotationally symmetric with a common symmetry axis, which may suggest that rotation has played a major role in their formation. The inner of the three rings is currently explained by the interaction of the blue supergiant wind with the wind of the red supergiant precursor (cf., Chevalier 1996). However, this interaction would result in a spherical shell in case of spherically symmetric winds. To understand the ring structure of the inner interaction region, and maybe also the two outer rings, significant rotation appears therefore to be required (cf. Martin & Arnett 1995), which may be provided by the spin-up mechanism. We may note that for this mechanism to work it is insignificant what actually triggered the blue loop; i.e. it would work as well for single star scenarios with a final blue loop (cf. Langer 1991a, Meyer 1997, Woosley et al. 1998) or for binary merger scenarios which predict a final red $\rightarrow$ blue transition of the merger star (cf. Podsiadlowski 1998).

We do not expect to find ring nebulae frequently around blue supergiants (cf. Brandner et al. 1997), since the time scale on which stars undergoing a blue loop shows very high surface rotation rates is rather small compared to the typical life time of a blue supergiant (cf. Langer 1991b), and because formed ring nebulae are quickly dissolved by the blue supergiant wind. SN 1987A is an exception, since here the transition to the blue happened only short time ago (i.e. the supernova exploded only shortly after the transition). However, the B[e] stars show emission line features which might be due to a circumstellar disk (cf. Zickgraf et al. 1996). The location of the less luminous subgroup of B[e] stars in the HR diagram (Gummersbach et al. 1995; cf. also de Winter & van den Ancker 1997) is in fact consistent with a blue loop scenario for their evolution. I.e., their disks might be produced by the spin-up mechanism described here (cf. also Langer & Heger 1998).

4. Conclusions

We have seen that rotation does affect the internal structure, evolution, surrounding and fate of massive stars. Rotationally induced mixing of matter shifts and disperses the mass-luminosity relation for massive main sequence stars. Their luminosity depends on mass *and* initial rotation rate. Stellar masses obtained from observed luminosities through standard M-L relations will in general result in too large masses (cf. Herrero et al. 1992). One consequence is that initial mass functions which are derived from observed luminosity functions using a mass-luminosity relation for non-rotating stars will systematically overestimate the number of the more massive stars. Furthermore, if the distribution of initial rotation velocities is not strongly peaked, the tracks shown in Figs. 3 and 5 demonstrate that the concept of isochrones in the HR diagram changes its character. Due to the dependence of the tracks on the initial rotation rate, isochrones are no longer lines but become surfaces in the HR diagram.

The rotational mixing of chemicals also affects the chemical yields of massive stars. The mixing on the main sequence, which is confirmed by many observations (cf Sect. 2.1), affects the production of light elements, the secondary CNO isotopes, sodium and the radio-nuclide ^{26}Al (cf. Langer et al. 1997b). It leads to larger core masses and lowers the lower mass limit for core collapse supernovae (cf. Fig. 5, and Sect. 2.3).

The transport of angular momentum can bring stars close to the Ω-limit of critical rotation. Very massive stars may thus arrive at critical rotation during core hydrogen burning. As the evolutionary time scale is long, this may be without dramatic consequences for the stars; possibly, the luminous B[e] stars are in that state (cf. Langer & Heger 1998). In any case, the amount of mass lost by these stars is depending on their initial rotation rate (cf. Sect. 3.2). This disperses the initial-final mass relationship: i.e., not only the core masses, but also the final stellar mass is not only a function of the metallicity, but a function of the initial rotation rate as well.

After core hydrogen exhaustion, very massive stars may hit the Ω-limit again, undergoing strong eruptions as a consequence of the short evolutionary time scale, shedding bipolar circumstellar nebulae (cf. Sect. 3.3). Less massive stars are spun-up on blue loop excursions from the Hayashi line. There rotation accelerates by much more than what would be expected from their mere contraction (Heger &

Langer 1998). Certainly, the progenitor of the supernova 1989A has experienced such a spin-up. In how far this helped to shape the rings around this supernova remains still to be explored.

Many of these effects of rotation remain quantitatively to be explored. However, for most of them there is overwhelming observational evidence showing their qualitative significance. There is no doubt that the initial rotation rate is a fundamental parameter for massive stars, which is equally important as the initial mass and metallicity.

Acknowledgements

The authors are very grateful to Peter Conti, André Maeder, Stan Owocki, Philipp Podsiadlowski, Regina Schulte-Ladbeck, and Franz-Josef Zickgraf for enlightening discussions. This work has been supported by the Deutsche Forschungsgemeinschaft through grant No. La 587/15-1

References

Aksenov A G, Zabrodina E A, Imshennik V S and Nadezhin D K 1997 *Astronomy Letters* **23** 677
Arnett W.D., Bahcall J.N., Kirshner R.P., Woosley S.E., 1989, ARAA 27, 629
Bjorkman J.E., Cassinelli J.P. 1993, ApJ 409, 429
Bohannan B., 1997, in *Luminous Blue Variables: Massive Stars in Transition*, A. Nota, H.J.G.L.M. Lamers, eds, ASP Conf. Ser., Vol. 120, p. 3
Brandner W., Grebel E.K., Chu Y.-H., Weis K., 1997, ApJ 475, L45
Bressan A., Fagotto F., Bertelli G., Chiosi C., 1993, A&AS 100, 47
Burrows, C.J., et al. 1995, ApJ, 452, 680
Carbon D., Barbuy B., Kraft R., Friel E., Suntzeff N., 1987, P.A.S.P. 99, 335
Chaboyer B., Zahn J.-P., 1992, A&A 253, 173
Chevalier, R.A. 1996, Ap&SS, 245, 255
Cowan J.J., Cameron A.G.W., Truran J.W., 1983 ApJ 265, 429
Crowther P.A., Smith L.J., Willis A.J., 1995, A&A 304, 269
Damineli A., Conti P.S. & Lopes D.F., 1997, New Astron. 2, 107
De Greve J.P., de Loore C., 1992 A&AS, 96, 653
de Koter A., Heap S.R., Hubeny I., 1997, ApJ 477, 792
de Winter D., van den Ancker M.E., 1997, A&AS 121, 275
Eddington A.S., 1925, Observatory 48, 73
Emden V.R., 1907, *Gaskugeln*, Leipzig
Endal A.S., Sofia S., 1978, ApJ 220, 279
Fliegner J., Langer N. & Venn K., 1996, A& A 308, L13
Friend D.B., Abbott D.C., 1986, ApJ 311, 701
Fransson C., Cassatella A., Gilmozzi R., et al., 1989, ApJ 336, 429
Frank A., Balick B., Davidson K., 1995, ApJ, 441, L77
Fukuda I., 1982, PASP 94, 271
García-Segura G., Mac Low M.-M., 1995a, 455, 145
García-Segura G., Mac Low M.-M., 1995a, 455, 160
García-Segura G., Mac Low M.-M., Langer N., 1996a, A&A 305, 229
García-Segura G., Langer N., Mac Low M.-M., 1996b, A&A 316, 133
García-Segura G., Langer N., Mac Low M.-M., 1997, in *Luminous Blue Variables: Massive Stars in Transition*, A. Nota, H.J.G.L.M. Lamers, eds, ASP Conf. Ser., Vol. 120, p. 332
García-Segura, G., Langer, RóżyczkaN., Franco J., 1998, ApJ, submitted
Gies D.R., Lambert D.L. 1992, ApJ, 387, 673
Gummersbach C.A., Zickgraf F.-J., Wolf B., 1995, A&A 302, 409
Han Z., Podsiadlowski P., Eggleton P.P., 1995, MNRAS, 272, 800
Heger A., Langer N., 1996, A&A 315, 421
Heger A., Langer N., 1998, A&A, in press
Heger A., Jeannin L., Langer N., Baraffe I., 1997, A&A 327, 224
Heger A., Woosley S.E., Langer N., 1998, ApJ, in preparation
Herrero A., Kudritzki R.P., Vilchez J.M., et al., 1992, A& A 261, 209
Howarth I.D., Siebert K.W., Hussain G.A.J., Prinja R.K., 1997, M.N.R.A.S. 284, 265
Huppert H.E., Turner J.S., 1981, J. Fluid Mech. 106, 299

Iben I. Jr., 1974, ARAA 12, 215
Ignace, R., Cassinelli, J.P., Bjorkman, J.E., 1996, ApJ, 459, 671
Kato S., 1966, PASJ 18, 374
Kippenhahn R., Weigert, A., 1990, Stellar Structure and Evolution, Springer, Berlin
Korycansky D.G., 1991, ApJ 381, 515
Laird D., 1985, ApJ 289, 556
Langer N., 1991a, A&A 243, 155
Langer N., 1991b, A&A 252, 669
Langer N., 1991c, A&A 248, 531
Langer N., 1992, A&A 265, L17
Langer N., 1994, in Proc. 34^{th} Herstmonceux Conference on *Circumstellar Media in the Late Stages of Stellar Evolution*, R. Clegg et al., ed., Cambridge University Press, p. 1
Langer N., 1997, in *Luminous Blue Variables: Massive Stars in Transition*, A. Nota, H.J.G.L.M. Lamers, eds, ASP Conf. Ser., Vol. 120, p. 332
Langer N., 1998, A&A, 329, 551
Langer N., Maeder A. 1995, A&A 295, 685
Langer N., Heger A., 1998, in proc. *Workshop on B[e] stars*, Paris 1997, C. Jaschek, A. M. Hubert, (eds.), Kluwer, in press
Langer N., Sugimoto D., Fricke K.J., 1983, A&A 126, 207
Langer N., El Eid M.F., Fricke K.J., 1985, A&A 145, 179
Langer N., Kiriakidis M., El Eid M.F., Fricke K.J., Weiss A., 1988, A&A 192, 177
Langer N., El Eid, M.F., Baraffe I., 1989, A&A 224, L17
Langer N., Hamann W.-R., Lennon M., Najarro F., Pauldrach A.W.A., Puls J., 1994, A& A 290, 819
Langer N., Heger A., Fliegner J., 1997a, in proc. IAU-Symp. 189 on *Fundamental Stellar Properties: The Interaction between Observation and Theory*, T. R. Bedding, A. J. Booth and J. Davis, eds., Kluwer, Dordrecht, p. 343
Langer N., Fliegner J., Heger A., Woosley S.E., 1997b, Nucl. Phys. A, 621, 83c
Langer N., García-Segura G., Mac Low M.-M., 1998, ApJ, submitted
Leitherer C., Chavarria-K., C., 1987, A&A 175, 208
Lennon D.J., 1994, Space Sci. Rev. 66, 127
Maeder A., 1987, A&A 178, 159
Maeder A., 1995, A&A 299, 84
Maeder A., 1997, A&A 321, 134
Maeder A., Meynet G., 1996, A& A 313, 140
Martin, C.L., Arnett, D. 1995, ApJ, 447, 378
Meyer F., 1997, MNRAS 285, L11
Meynet G., Maeder A., 1997, A& A 321, 465
Meynet G., Maeder A., Schaller G., Schaerer D., Charbonnel C., 1994, A&AS 103, 97
Nota, A., Livio, M., Clampin, M., Schulte-Ladbeck, R. 1995, ApJ, 448, 788
Nota A., Smith L., Pasquali A., Clampin M. & Stroud M., 1997, ApJ 486, 338
Owocki S.P., Cranmer S.R., Gayley K.G., 1996, ApJ 472, L11
Pasquali A., Langer N., Schmutz W., Leitherer C., Nota A., Hubeny I., Moffat A.F.J., Drissen L., Robert C.: 1997, ApJ 478, 340
Penny L.R., 1996, ApJ 463, 737
Petrenz P., Puls J., 1996, A& A 312, 195
Plait, P.C., Lundquist, P., Chevalier, R.A., Kirshner, R.P. 1995, ApJ, 439, 730
Podsiadlowski P., 1998, in: *SN 1987A: Ten years after*, Eds. M.M. Phillips, N.B. Suntzeff, PASP, in press
Ritossa C, Garcia-Berro E and Iben I Jr 1996 Ap. J. **460** 489
Schaller G., Schaerer D., Meynet G., Maeder A. 1992, A&AS, 96, 269
Schönberner D., A. Herrero, K. Butler, S. Becker, F. Eber, R.P. Kudritzki and K.P. Simon, 1988, A&A 209, 197
Schulte-Ladbeck R., 1997, Rev. Modern Astron. 10, 135
Schulte-Ladbeck R., 1998, in proc. *Workshop on B[e] stars*, Paris 1997, C. Jaschek, A. M. Hubert, (eds.), Kluwer, in press
Schulte-Ladbeck R., Clayton G.C., 1993, AJ 106, 790
Schwarz, H.E., Corradi, R.L.M., Melnick, J. 1992, A&AS, 96, 23
Spruit H.C., 1998, A&A, in press
Spruit H.C., Knobloch E., 1984, A&A 132, 89
Stothers R.B., Chin C.-W., 1975, ApJ 198, 407
Stothers R.B., Chin C.-W., 1976, ApJ 204, 472
Stothers R.B., Chin C.-W., 1996, ApJ 468, 842
Talon S., Zahn J.-P., 1997, A& A 317, 749

Talon S., Zahn J.-P., Maeder A., Meynet G., 1997, A&A 322, 209
van Genderen A. M., de Groot M.J.H., & The P.S, 1994, A& A, 283, 89
Venn K.A., 1996, P.A.S.P. 108, 309
Venn K.A., Lambert D.L., Lemke M. 1996, A&A 307, 849
Walborn, N., in "Atmospheric Diagnostics of Stellar Evolution", proc. IAU-Symp. No. 108 (1988), K. Nomoto, ed., p. 70.
Weaver R., McCray R., Castor J., Shapiro P., Moore, 1977, ApJ 218, 377
Weaver T.A., Zimmerman G.B., Woosley S.E., 1978, ApJ 225, 1021
Weis K., Duschl W.J., Bomans D.J., Chu Y.-H., Joner M.D., 1997, A& A, 320, 568
Woosley, S.E., Heger, A., Weaver, T.A., Langer, N., 1998, in: *SN 1987A: Ten years after*, Eds. M.M. Phillips, N.B. Suntzeff, PASP, in press
Yamada S and Sato K 1994 Ap. J. **434** 268
Zahn J.-P., 1983, in proc. 13th Saas-Fee Course, A. Maeder et al., eds., Geneva Observatory
Zahn J.P., 1992, A&A, 265, 115
Zahn J.P., 1994, in: *Evolution of Massive Stars: A Confrontation between Theory and Observations*, D. Vanbeveren et al., eds., Kluwer, Dordrecht, p. 285
Zickgraf F.J., Humphreys R.M., Lamers H.J.G.L.M., Smolinski J., Wolf B., Stahl O., 1996a, A&A 315, 510
Zickgraf F.J., Kovács J., Wolf B., Stahl O., Kaufer A., Appenzeller I., 1996b, A&A 309, 505